



RESEARCH PAPER



Development and multimodal characterization of an elastase-induced emphysema mouse disease model for the COPD frequent bacterial exacerbator phenotype

Irene Rodríguez-Arce^a, Xabier Morales^{b,c}, Mikel Ariz^{b,c}, Begoña Euba ^a, Nahikari López-López^a, Maider Esparza^{b,c}, Derek W. Hood^d, José Leiva^{e,f}, Carlos Ortiz-de-Solórzano^{e,b,c}, and Junkal Garmendia ^{g,a}

^aInstituto De Agrobiotecnología, CSIC (IdAB-CSIC)-Gobierno de Navarra, Mutilva, Spain; ^bDepartment of Solid Tumors and Biomarkers, Center for Applied Medical Research (CIMA), Laboratory of Preclinical Models and Analytical Tools, Pamplona, Spain; ^cLaboratory of Preclinical Models and Analytical Tools, Division of Solid Tumors and Biomarkers, Center for Applied Medical Research (CIMA), Pamplona, Spain; ^dMammalian Genetics Unit, MRC Harwell Institute, Oxfordshire, UK; ^eInstituto De Investigación Sanitaria De Navarra (IdiSNA), Pamplona, Spain; ^fServicio De Microbiología, Clínica Universidad De Navarra, Pamplona, Spain; ^gCentro De Investigación Biomédica En Red De Enfermedades Respiratorias (CIBERES), Madrid, Spain

ABSTRACT

Chronic obstructive pulmonary disease (COPD) patients undergo infectious exacerbations whose frequency identifies a clinically meaningful phenotype. Mouse models have been mostly used to separately study both COPD and the infectious processes, but a reliable model of the COPD frequent exacerbator phenotype is still lacking. Accordingly, we first established a model of single bacterial exacerbation by nontypeable *Haemophilus influenzae* (NTHi) infection on mice with emphysema-like lesions. We characterized this single exacerbation model combining both non-invasive *in vivo* imaging and *ex vivo* techniques, obtaining longitudinal information about bacterial load and the extent of the developing lesions and host responses. Bacterial load disappeared 48 hours post-infection (hpi). However, lung recovery, measured using tests of pulmonary function and the disappearance of lung inflammation as revealed by micro-computed X-ray tomography, was delayed until 3 weeks post-infection (wpi). Then, to emulate the frequent exacerbator phenotype, we performed two recurrent episodes of NTHi infection on the emphysematous murine lung. Consistent with the amplified infectious insult, bacterial load reduction was now observed 96 hpi, and lung function recovery and disappearance of lesions on anatomical lung images did not happen until 12 wpi. Finally, as a proof of principle of the use of the model, we showed that azithromycin successfully cleared the recurrent infection, confirming this macrolide utility to ameliorate infectious exacerbation. In conclusion, we present a mouse model of recurrent bacterial infection of the emphysematous lung, aimed to facilitate investigating the COPD frequent exacerbator phenotype by providing complementary, dynamic information of both infectious and inflammatory processes.

ARTICLE HISTORY

Received 14 December 2020
Revised 20 May 2021
Accepted 30 May 2021





KEYWORDS


Lung emphysema; bacterial exacerbation; inflammation; test of pulmonary function; micro-CT

Introduction

Chronic obstructive pulmonary disease (COPD) is a clinical syndrome characterized by chronic respiratory symptoms, structural pulmonary abnormalities (airway disease, emphysema, or both), lung function impairment (poorly reversible airflow limitation), or any combination of these [1]. COPD patients undergo episodes of acute deterioration in respiratory health termed exacerbations, described as the acute worsening of respiratory symptoms associated with a variable degree of physiological deterioration. Exacerbations are associated with increased systemic and airway

inflammation, worsening of lung function (according to post-bronchodilator FEV1), greater impairment in health status (quality of life), and increased white-cell count [2,3]. Most exacerbations have an infectious origin and are triggered by respiratory bacterial and viral infections. Approximately one half of these infectious exacerbations are triggered by bacteria, whereas the other half is triggered by viral infections [4]. In particular, bacterial exacerbations are characterized by increased dyspnea and sputum production, and by changes in the sputum color [5]. *Haemophilus influenzae*, in its nontypeable (NTHi) form, is one of the most common bacterial species isolated from respiratory

CONTACT Junkal Garmendia  juncal.garmendia@csic.es  Instituto de Agrobiotecnología, CSIC-Gobierno de Navarra, 31192 Mutilva, Navarra, Spain; Carlos Ortiz de Solórzano  codesolorzano@unav.es  Laboratory of Preclinical Models and Analytical Tools, Division of Solid Tumors and Biomarkers, Center for Applied Medical Research, Pamplona, Spain

 Supplemental data for this article can be accessed [here](#)

© 2021 The Author(s). Published by Informa UK Limited, trading as Taylor & Francis Group.

This is an Open Access article distributed under the terms of the Creative Commons Attribution-NonCommercial License (<http://creativecommons.org/licenses/by-nc/4.0/>), which permits unrestricted non-commercial use, distribution, and reproduction in any medium, provided the original work is properly cited.

samples in COPD exacerbations [6–11]. One clinically meaningful COPD phenotype is termed frequent exacerbator, characterized by the occurrence of two or more exacerbations per year [1,2,12]. Frequent exacerbations lead to increased risk of depressive symptoms, decline in lung function, poorer quality of life, decreased physical activity, increased health-care utilization, and up to a threefold increase in mortality [12].

Animal models allow investigating the pathobiology of a disease, to anticipate the value of biological markers, and can be used as platforms for in-depth analysis of possible therapeutic intervention of pathways involved in the disease. As long-term exposure to cigarette smoke is a main risk for COPD, cigarette smoke murine models have been used on their own or combined with inactivated NTHi bacteria, to study the disease [13–15]. However, the complexity of these models, and the difficulty to faithfully reproduce the heterogeneity of COPD, has shifted the focus of animal models toward one of its hallmarks, parenchymal lung tissue destruction by neutrophil-produced elastase, resulting in pulmonary fibrin deposition and decreased lung volume. Indeed, mice treated with elastase exhibit lung damage consistent with several COPD features, including parenchymal collapse, enlargement of airspaces, and fibrotic deposits within the lung alveolar spaces [16]. The clinical relevance of infectious COPD exacerbations has also promoted the use of animal models of bacterial (NTHi, *Streptococcus pneumoniae*, *Staphylococcus aureus*) or viral (flu virus) infection-induced exacerbations, showing that infections increase inflammation, remodeling, and emphysema, and that COPD increases susceptibility to respiratory infection [17]. Regarding NTHi, pulmonary infection in cigarette smoke-exposed or emphysematous mice, and in emphysematous hamsters [16,18–22] has been reported. However, despite its relevance, animal models resembling features of the COPD frequent exacerbator phenotype are currently lacking. Here, we report the development and longitudinal, multimodal characterization of a disease model based on recurrent NTHi pulmonary infection of a murine emphysematous lung, which could be of use to obtain novel insights on the COPD frequent exacerbator phenotype and its response to therapies.

Microbial load quantification by colony-forming units (CFU) count after tissue homogenization and serial dilution plating, and microscopic observation of infected tissue sections, are the gold standard techniques used to evaluate infections in small animal models [23]. Based on our prior experience quantifying lung damage in an elastase-induced mouse model of emphysema [24–27], here we put forward the notion that

modeling bacterial exacerbations will also benefit from the use of noninvasive *in vivo* techniques to study the dynamic process of infection, thus obtaining longitudinal, correlative information about the extent of both lung damage and microbial load. This involves a multimodal approach that combines pulmonary function tests (PFT) to quantify alterations of the pulmonary physiology, with noninvasive micro-computed X-ray tomography (micro-CT), for the longitudinal visualization and quantification of imaging-derived biomarkers such as the lung tissue volume, low-density areas typical of emphysema, or ground-glass opacity regions associated to inflammation [23,28]. In summary, we present a multimodal, longitudinal characterization of the bacterial dynamics and host responses to emphysema lung infection by NTHi when occurring in an acute or repeated manner, and show its utility for antimicrobial efficacy testing.

Methods and materials

Animal handling

The assays performed are described next and the Methods used in each assay are detailed in the Supplementary Material.

A. NTHi infection conditions (pilot assay). Eighty-four CD1 female mice were randomly divided into four groups: (i) intranasally infected with stationary grown NTHi RdKW20; (ii) intranasally infected with stationary grown NTHi Xen21; (iii) intranasally infected with exponentially grown Xen21; (iv) oropharyngeally infected with exponentially grown Xen21. Mice in each group ($n = 7$) were sampled 12, 24, and 30 hours post-infection (hpi) and underwent lung processing for CFU counts.

B. NTHi infection in an emphysematous background to model COPD bacterial exacerbation. Two assays were performed. In the first one, aimed at determining the baseline effect of the emphysematous background in the bacterial load, 94 CD1 female mice were divided into four groups: (i) mice instilled with a vehicle solution (V+/I-); (ii) mice instilled with a vehicle solution, NTHi infected (V+/I+); (iii) mice with lung emphysema (E+/I-); (iv) mice with lung emphysema, NTHi infected (E+/I+). Mice in each group (V+/I- and E+/I-, $n = 5$; V+/I+ and E+/I+, $n = 5$) were sampled 6, 12, 24, 30, and 48 hpi, and 1 week post-infection (wpi). In detail, V+/I+ and E+/I+ groups were sampled 6, 12, 24, 30, and 48 hpi and underwent lung processing for CFU counts; mice from all groups were sampled for gene expression and histopathology analyses 24 and 48 hpi, and 1 wpi. In

the second assay, aimed at complementing the *ex vivo* made measurements with *in vivo* longitudinal evaluation of pulmonary function and radiological status, 50 CD1 female mice were divided into five groups: (i) healthy control mice (CON); (ii) mice instilled with a vehicle solution (V+/I-); (iii) mice with lung emphysema (E+/I-), and NTHi infected groups as those in the first assay, (iv) V+/I+ and (v) E+/I+. Mice in each group (n = 10) were sampled as follows: (i) 24 and 48 hpi, 1, 2, and 3 wpi, all animals underwent PFT, and at least 3 mice per group underwent micro-CT imaging; (ii) 1, 3, 6, 9, 12, and 24 hpi, bioluminescence was measured.

C. NTHi recurrent infection in an emphysematous background to model COPD frequent exacerbation. Three separate assays were performed. In all three assays, the infected groups were infected twice (I2+). The first infection was performed 17 days (d) after vehicle solution or elastase administration; re-infection was performed 24 d after vehicle solution or elastase administration. In the first assay, aimed at determining the baseline effect of the emphysematous background in bacterial load after recurrent infection, 56 CD1 female mice were randomly divided into two groups: (i) V+/I2+; (ii) E+/I2+. In the second assay, aimed at completing the measurements of bacterial load in the frequent exacerbation phenotype with *in vivo* evaluation of pulmonary function and the radiological status, 28 CD1 female mice were randomly divided into four groups: (i) V+/I2-; (ii) E+/I2-; (iii) V+/I2+; (iv) E+/I2+. In the third assay, aimed at determining the clearing effect of azithromycin dehydrate (AZM) treatment in mice after recurrent infection, 84 CD1 female mice were randomly divided into four groups: (i) mice instilled with a vehicle solution, NTHi infected, and treated with water, vehicle solution where the macrolide dissolves (V+/I2+); (ii) mice instilled with a vehicle solution, NTHi infected, and treated with AZM (V+/I2+/AZM); (iii) mice with lung emphysema, NTHi infected, and water treated (E+/I2+); (iv) mice with lung emphysema, NTHi infected, and AZM treated (E+/I2+/AZM). In this first assay, mice in each group (n = 7) were sampled 24, 48, 72, and 96 h post re-infection, underwent lung processing for CFU counts, and samples were also collected for histopathology analyses. In the second assay, mice in each group (n = 7) underwent PFTs 24 and 48 h, and 1, 2, 3, 6, 9, and 12 weeks post re-infection, and at least two animals per group underwent micro-CT thoracic imaging. In the third assay, mice in each group (n = 7) were sampled 24, 30, and 36 h post re-infection and underwent lung processing for CFU counts.

Results

Multimodal dynamic analysis of a model of COPD exacerbation by bacterial infection in a murine emphysematous lung

The protocol used for the generation and longitudinal analysis of a mouse model of infectious exacerbation (E+/I+) is presented in [Figure 1a](#) that shows all the assays performed and sampling time points. We next describe the E+/I+ model and its controls, i.e. the emphysema only (E+/I-) and respiratory infection only (V+/I+) models.

Emphysema model (E+/I-)

To elicit pulmonary damage consistent with emphysema, mice were treated with pancreatic porcine elastase (PPE) delivered via nonsurgical oropharyngeal instillation. As previously reported [18,24], emphysema-like patho-physiological features were confirmed 17 d after elastase instillation, while vehicle-treated mice (V+/I-) displayed pulmonary function parameters similar to those of control mice with normal lung function (CON). Specifically, elastase-treated mice (E+/I-) showed significant decrease in resistance (R) and elastance (E), and increased compliance (C) at all time points tested (**Figure S1A-C**). Similarly, the complex, broadband-forced oscillation model revealed significantly lower airways (Rn) as well as parenchymal resistance (G), reduced tissue elasticity (H), and a significant increase in tissue resistance to airflow deformation (inertance, I) compared to vehicle-treated (V+/I-) and control (CON) mice, at all times tested (**Figure S1D-G**). These values confirm an abnormal distension of alveolar lung parenchyma and the lung airway walls during tidal breathing, as well as impaired elastic recoil of the parenchyma. Altogether, they suggest that the instillation of elastase elicits a reduction in airflow resistance, caused both by pathological changes in the central airways and lung tissue, consistent with elastolytic parenchymal degradation and airway remodeling. Furthermore, visual analysis of micro-CT image scans revealed lower X-ray density, and swollen lungs in E+/I- animals compared to the V+/I- and CON groups (**Figure S1H-I**). These observations were further confirmed by automatic quantification of the micro-CT scans. Indeed, quantified lung volumes were significantly higher in E+/I- compared to V+/I- and CON animals (**Figure S1J**). Moreover, lung volumes in E+/I- mice increased over time contrasting with the flat, constant trend measured in both V+/I- and CON groups. Regarding the extent of emphysema, measured as the percentage of lung voxels below -900 Hounsfield units (RVB -900 HU) [24], the obtained values were

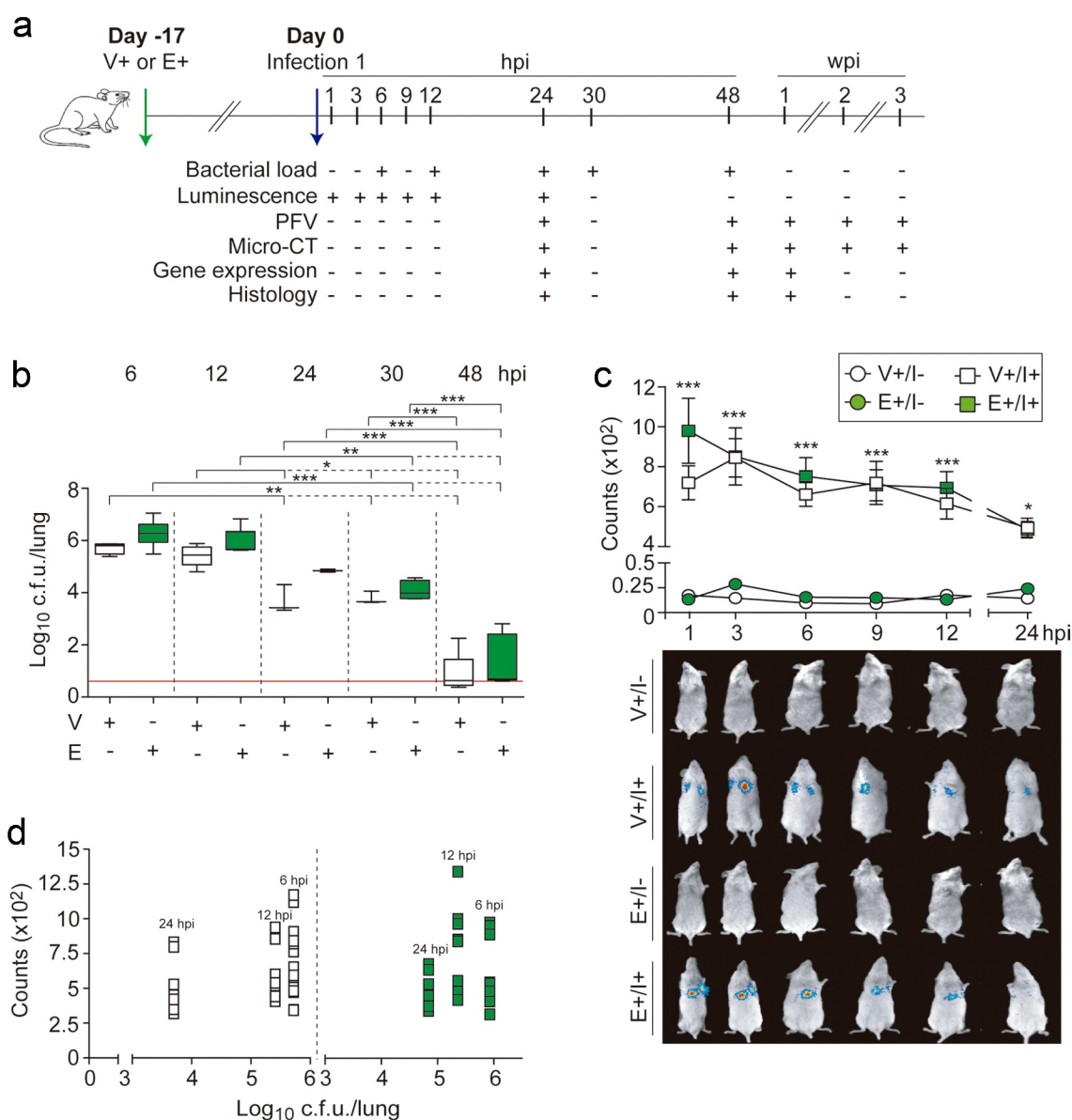


Figure 1. A mouse model of lung emphysematous infection: experimental design and characterization. (a) Experimental design: lung emphysema was induced by oropharyngeal instillation of PPE in CD1 mice (Day -17). Elastase instillation induces pulmonary damage compatible with emphysema-like lesions. Mice were instilled with PPE (E+/-) or received physiological saline solution (V+/-). Animals were infected with $\sim 10^8$ CFU/mouse of *H. influenzae* Xen21 (Day 0), V+/- and E+/- groups. Assay types and sampling time points are indicated. (b) Longitudinal analysis of lung bacterial loads. Mice were infected as indicated in (a), euthanized 6, 12, 24, 30 and 48 hpi, and bacterial loads quantified in homogenized lungs. No significant differences were observed between V+/- (white) and E+/- (green) groups at any of the indicated time points. V+/- groups: bacterial counts were lower 24, 30 and 48- than 6 hpi ($p < 0.005$); bacterial counts were lower 24, 30 and 48- than 12 hpi ($p < 0.05$); bacterial counts were lower 48- than 24 and 30 hpi ($p < 0.0001$). E+/- animals: bacterial counts were lower 30 and 48- than 6 hpi ($p < 0.0001$); bacterial counts were lower 30 and 48- than 12 hpi ($p < 0.005$); bacterial counts were lower 48- than 24 and 30 hpi ($p < 0.0001$). Results are reported as \log_{10} CFU/lung and represented as box plot graphs (lines inside boxes represent median values). Statistical comparisons were performed using one-way ANOVA and Tukey's multiple comparison test. *** $p < 0.001$; ** $p < 0.01$; * $p < 0.05$. (c) Bacterial bioluminescence was determined 1, 3, 6, 9, 12 and 24 hpi, representative animals are shown (bottom panel). Results are shown as mean \pm SEM. Statistical comparisons were performed using one-way ANOVA and Tukey's multiple comparison test. *** $p < 0.001$; * $p < 0.05$. (d) *H. influenzae* Xen21 light levels and bacterial numbers *in vivo*. Bacterial counts and animal luminescence determined at different time points post-inoculation (6, 12 and 24 h). Spearman's correlation coefficient was determined.

significantly higher in E+/I- compared to V+/I- and CON mice, suggesting the prevalence of low X-ray density areas, consistent with emphysema-like lesions (**Figure S1K**). Accordingly, Mean Lung Voxel Intensity (MLVI) values, that describe the average intensity of the lung in HU, and are expected to be lower in emphysematous compared to healthy lungs, were lower in E+/I- than in V+/I- and CON mice (**Figure S1L**). These results are clearly reflected in the 3D volume renders shown in **Figures S1M, 3e, and 3j**.

Histological images of lung sections were also analyzed 24 d after elastase instillation, to measure the main histopathological descriptors of emphysema (i.e. the alveolar space, measured through the mean linear intercept (MLI), a weighted mean measure of alveolar size (D2), and the ratio of alveolar space with respect to the whole lung tissue ($R_{\text{alv/tissue}}$). The five lung lobes were quantified independently. All three parameters were significantly higher in E+/I- than in V+/I-, confirming the presence of emphysema. No significant differences were found between lobes, meaning that the presence of emphysema was homogeneous across the lung (**Figure S2**). Caspase-3 staining on these same lungs revealed a clear, though not statistically significant increase in apoptotic cell density (Caspase-3⁺/mm² ($p > 0.075$) in mice treated with elastase (E+/I-) compared to control (V+/I-) mice (**Figure S3**). These results suggest that elastase treatment elicits the apoptosis of alveolar cells. This is consistent with the parenchymal destruction and airspace enlargement observed in IHC by H&E sections (**Figure S2**), and the low lung X-ray density observed in the micro-CT images (**Figure S1I-L**).

Furthermore, matrix metalloproteinases (MMPs), which are crucial for extracellular matrix remodeling following tissue damage, and are elevated in sputum, bronchoalveolar lavage, and lung tissue specimens from animals and patients with COPD [29,30], were quantified in our models. Notably, the expression of the *mmp-2* and *mmp-12* genes in emphysematous (E+/I-) lungs was higher than in control (V+/I-) uninfected lung tissue (**Figure S4C-D**).

Altogether, these findings demonstrate degradation of the alveolar walls and enlargement of the airspace induced by elastase activity, which strongly agrees with the physiological parameters detected by PFT.

Respiratory infection model (V+/I+)

The *H. influenzae* RdKW20 strain has been previously used in mouse models of lung infection [31,32]. Both RdKW20 and Xen21 (RdKW20 derivative with a *luxCDABE* insert [33]) strains showed similar growth dynamics, while Xen21 bioluminescence accurately reflected the measured bacterial numbers (**Figure**

S5A). Likewise, RdKW20 and Xen21 lung bacterial counts were comparable upon CD1 mice intranasal infection, supporting our use of Xen21 for subsequent experiments (**Figure S5B**). Lung infection with similar inocula of exponential or stationary phase grown Xen21 bacteria rendered comparable results, although lower variability was observed in the counts obtained when using exponentially grown bacteria (**Figure S5C**). Finally, we compared lung bacterial loads after intranasal or oropharyngeal administration, obtaining similar results. However, the bioluminescent signal detected in the lungs of oropharyngeally infected mice was higher than the one obtained in the lungs of intranasally infected animals (**Figure S5D**). Together, these results supported our use of oropharyngeal administration of the exponentially grown *H. influenzae* strain Xen21 to generate a mouse model of lung infection.

Bacterial loads were quantified in V+/I+ lungs. Bacterial counts remained comparable 6 and 12 hpi ($\sim 10^6$ CFU/lung), decreased reaching a second plateau between 24 and 30 hpi ($\sim 10^4$ CFU/lung), and became barely detectable 48 hpi (**Figure 1b**). In parallel, we used bacterial bioluminescence for real-time noninvasive detection of NTHi dynamics *in vivo*. Here, the lungs of infected mice were found to emit low bioluminescent signals ($6\text{--}10 \times 10^2$ photonic counts), decreasing with time as expected (**Figure 1c**). However, no significant correlation coefficients (Spearman $r = 1$ in V+/I+ mice) were found between photon counts and bacterial loads at the sampled times (**Figure 1d**). Furthermore, isolated lung lobes of the same mice exhibited also low bioluminescence signals (data not shown), altogether suggesting that bioluminescence emission was not a good indicator of NTHi pulmonary infection in this model.

The dynamics of pulmonary infection by *H. influenzae* were also examined by PFT and micro-CT. During the first 48 hpi, PFT values obtained by single-frequency-forced oscillation revealed that V+/I+ lungs display higher resistance (R) and elastance (E) and lower compliance (C), compared to non-infected V+/I- and CON mice. However, these differences disappear 1 week after infection, consistent with the remission of the effects of the infection (**Figure 2a-c**). Similarly, PFT values obtained using a broadband-forced maneuver revealed a significant decrease in tissue inertance (I), compared to non-infected mice during the first 48 h, suggesting an increment of parenchymal rigidity. On the contrary, tissue elasticity (H) displayed significantly higher values during the first 48 h compared to non-infected mice. Likewise, airways (Rn) and parenchymal (G) resistance were also higher in V+/I+ compared to V+/I- and CON mice 24 and 48 hpi, consistent with the higher stiffness of both

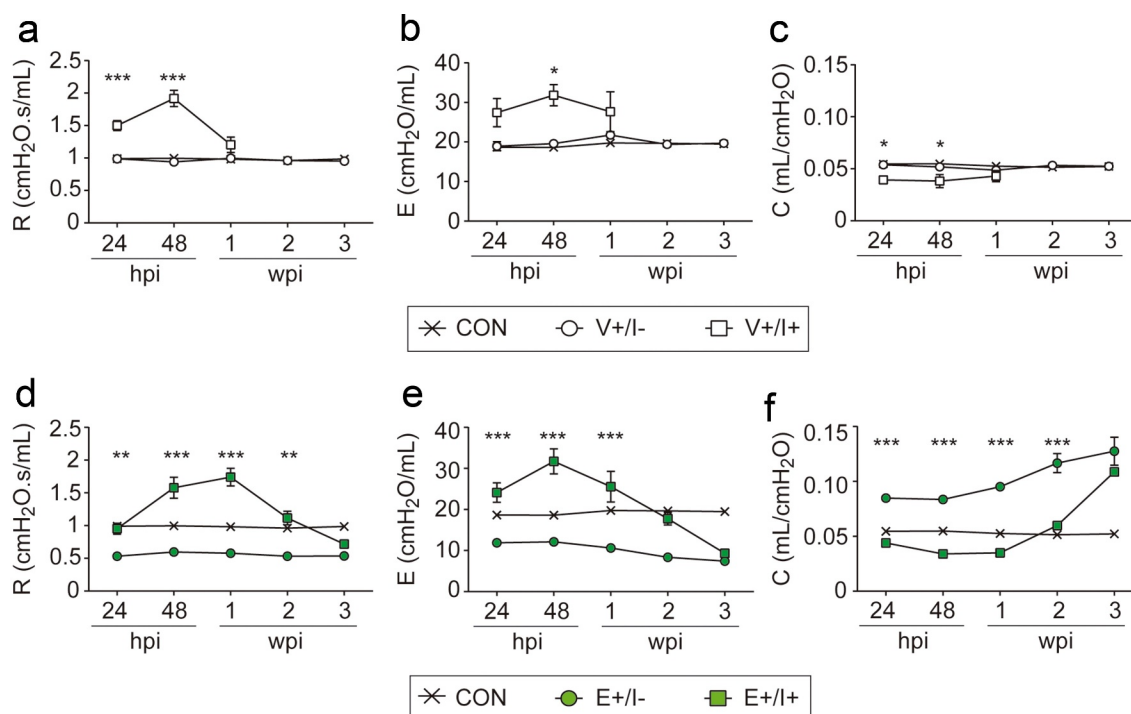


Figure 2. Pulmonary NTHi infection modifies lung physiology in the murine model. Evolution of pulmonary physiological parameters at the indicated post-infection time points by PFT (24 and 48 hpi; 1, 2 and 3 wpi). Mice groups: non-infected control animals with normal lung function (CON, black cross); V+/- and E+/-, white and green circles, respectively; V+/+ and E+/+, white and green squares, respectively. (a and d) Lung resistance (R, cmH₂O.s/mL), (b and e) elastance (E, cmH₂O/mL), (c and f) compliance (C, mL/cmH₂O), measured by the single-frequency forced oscillation maneuver. Results are shown as mean \pm SEM, statistical differences were analyzed using a two-way ANOVA followed by Bonferroni's post-hoc test. *** $p < 0.001$; ** $p < 0.01$; * $p < 0.05$.

compartments (Figure S6, upper panels). These results suggest altered pulmonary function as early as 24 hpi, worsening 48 hpi, when the parenchyma displays lower distention capacity and increased level of resistance, i.e. constriction in the lungs, both in the airways and alveolar areas, that recovers 1 week after infection. Visual analysis of micro-CT images reveals evident inflammatory signs 24 and 48 hpi in all lung lobes (Figure 3a). Indeed, chest scans showed densely radiopaque areas, as well as consolidated and ground-glass opacity regions, which disappear 1 week after infection. This observation was confirmed by quantification of the corresponding micro-CT images. In particular, the MLVI parameter, indicative of the parenchymal opacity compatible with the inflammatory process, increased significantly 48 hpi, as also observed in the three-dimensional reconstruction (Figure 3d-e). Finally, as expected, no significant differences in total lung volume and RVB -900 HU were detected among groups (Figure 3b-c). These results reveal parenchymal obstruction happening during the first 48 h after infection, disappearing 1 wpi, confirming the alterations in pulmonary physiology detected by PFT.

For completion, inflammation was also analyzed at the molecular level. The expression of *kc* and *tnf- α* pro-

inflammatory mediators in lung tissue of V+/+ mice was higher 24 and 48 hpi than in non-infected V+/- animals, and this increase was restored to basal levels 1 wpi. In contrast, the expression of the *mmp-2* and *mmp-12* genes in lung tissue of V+/+ mice was lower at 24 and 48 hpi than in V+/- animals, and such decrease was restored to basal levels 1 wpi (Figure S4). A microscopy-based score of the lower airway histopathological lesions in samples from infected mice was also quantified. No significant differences in terms of lymphocyte counts were observed between V+/- and V+/+ groups. In contrast, scoring of alveolar macrophages and bronchiolar recruitment of polymorphonuclear cells (PMN) showed higher numbers in V+/+ than in V+/- animals. PMN recruitment was higher 24 and 48 hpi, and decreased after 1 wpi (Table 1, upper panels). In summary, the inflammatory response, measured by the expression of pro-inflammatory cytokines and recruitment of PMNs and macrophages nicely correlates with the damage quantified by means of PFT and radiological measurements.

Model of COPD bacterial exacerbation by single-dose NTHi infection in emphysematous mice (E+/+)

COPD bacterial exacerbation was elicited by oropharyngeal administration of exponentially grown

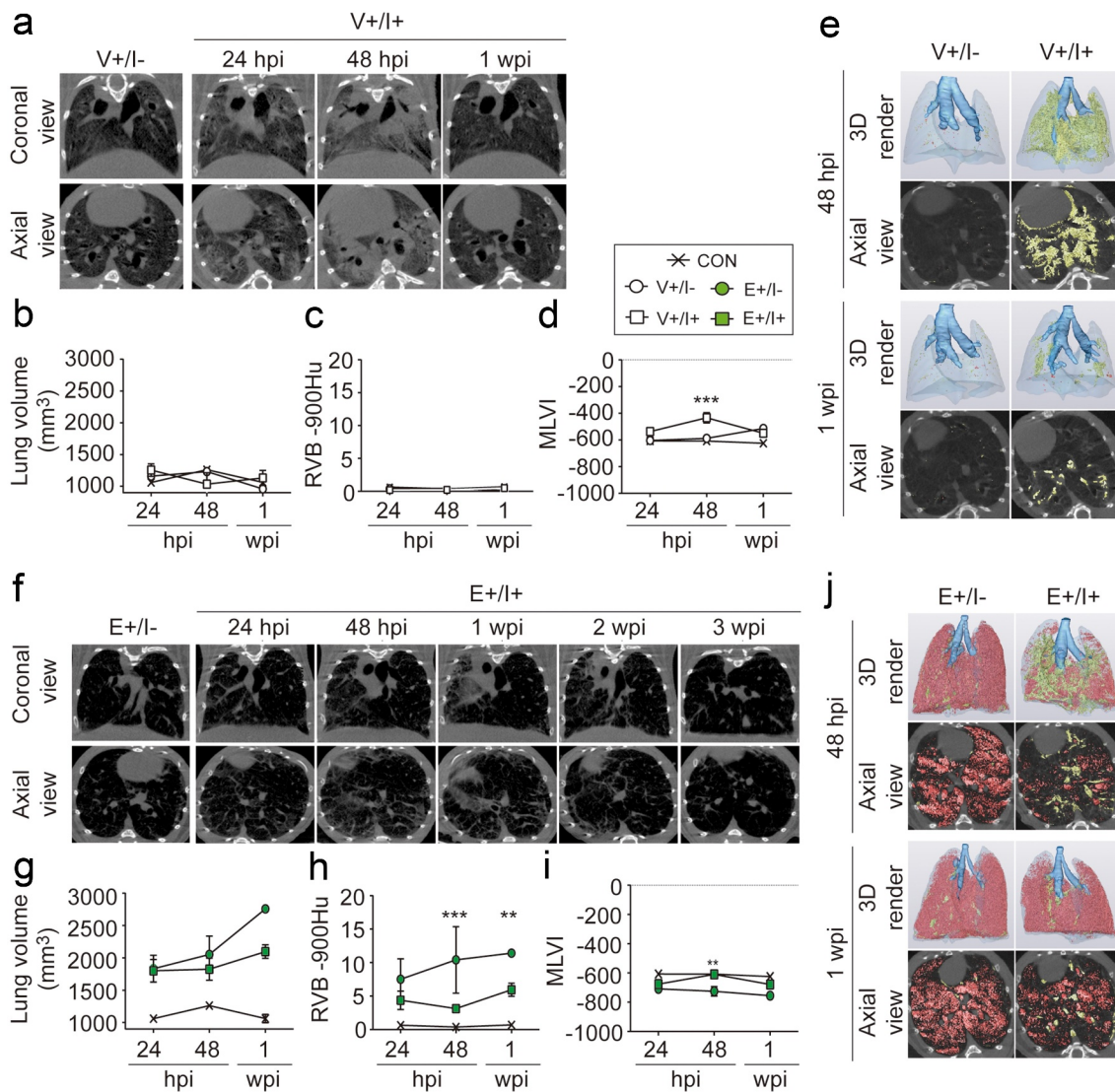


Figure 3. Pulmonary NTHi infection induces lung inflammation in the murine model. (a and f) Representative micro-CT images in the longitudinal section (upper row) and cross-section (bottom row) acquired from the chest of the V+/- and V+/+ (a), and E+/- and E+/+ (f) mice, at the indicated time points. Evolution of the image parameters calculated from the micro-CT scans at the indicated time points (number of images, $n \geq 3$). Mice groups: non-infected control animals with normal lung function (CON, black cross); V+/- and E+/-, white and green circles, respectively; V+/+ and E+/+, white and green squares, respectively. (b and g) Total lung volume (mm³). (c and h) Relative lung volume below -900 HU (RVB -900 HU). (d and i) Mean lung voxel intensity (MLVI). (e) Representative rendered views, and 2D axial micro-CT slices of a lung from V+/- and V+/+ models, 48 hpi and 1 wpi. Yellow areas indicate hyperintense regions corresponding with infection. (f) Representative 3D rendered views, and 2D axial micro-CT slices of a lung from E+/- and E+/+ models, 48 hpi and 1 wpi. Yellow areas indicate hyperintense regions corresponding with infection. Red areas indicate areas of low X-ray absorption corresponding with emphysema. In (e) and (j), lung reconstructions show the main airways in solid blue, the lungs in transparent blue, the low-density areas in red (RVB -900 HU), and the high-density areas in yellow (RV -30/-150 HU). Axial micro-CT slices show RVB -900 HU and RV -30/-150 HU parameters merged on the radiographic image. Results are shown as mean \pm SEM, statistical differences were analyzed using a two-way ANOVA followed by Bonferroni's post-hoc test. *** $p < 0.001$; ** $p < 0.01$; * $p < 0.05$.

H. influenzae strain Xen21 in emphysematous mice. As observed in V+/- animals, bacterial counts remained comparable 6 and 12 hpi ($\sim 10^6$ CFU/lung), decreased reaching a second plateau between 24 and 30 hpi ($\sim 10^4$ CFU/lung), and became barely detectable 48 hpi. Even if the trend was similar, bacterial counts were consistently higher in E+/- than in V+/- groups

(Figure 1b). As indicated, the lungs of infected mice were found to emit very low bioluminescent signals (Figure 1c), resulting in no significant correlation coefficients (Spearman $r = 0.5000$ in E+/- mice) between photon counts and bacterial loads (Figure 1d).

PFT values obtained by single-frequency-forced oscillation revealed lower compliance (C) and higher

Table 1. Score of histopathology lesions found in the airways of V+ or E+ administered mice, infected with the strain *H. influenzae* Xen21.

| | | Score (mean ± SD) ^a | | | |
|---------------------|--------|--------------------------------|------------------------------|--------------------------|--------------------------|
| | | hpi | Bronchioli PMNs ^b | Alveolar macrophages | Lymphocytes |
| Single infection | V+/- | - | 0.2 ± 0.27 | 0 | 0 |
| | E+/- | - | 0.4 ± 0.25 | 0.5 | 0 |
| | V+/I+ | 24 | ^f 1.8 ± 0.5 | ^c 1 ± 0.3 | 0 |
| | | 48 | ^f 2.5 ± 0.4 | ^c 1.5 | 0.1 ± 0.4 |
| | | 168 (1 week) | ^f 1.1 ± 0.75 | ^c 1.3 ± 0.28 | 0 |
| Recurrent infection | E+/I+ | 24 | ^f 1.9 ± 0.5 | ^{c,d} 1.4 ± 0.2 | 0 |
| | | 48 | ^f 2.1 ± 0.4 | ^c 1.4 ± 0.2 | 0.4 ± 0.5 |
| | | 168 (1 week) | ^g 0.4 ± 0.39 | ^c 1.1 ± 0.41 | 0.4 ± 0.52 |
| | V+/I2+ | 24 | 1.25 ± 0.29 | ^e 1.38 ± 0.48 | 0.13 ± 0.25 |
| | | 48 | 1.63 ± 0.85 | ^e 1.38 ± 0.48 | 0.38 ± 0.48 |
| | | 72 | 0.75 ± 0.65 | ^e 2 ± 0.71 | ^h 1 ± 0.41 |
| | | 96 | 0.5 ± 0.7 | ^e 2.25 ± 0.35 | ^h 1.5 |
| | E+/I2+ | 24 | 1 ± 0.84 | ^e 1.42 ± 0.58 | 0.33 ± 0.26 |
| | | 48 | 0.25 ± 0.86 | ^e 2 ± 0.74 | ^h 0.75 ± 0.27 |
| | | 72 | 0.25 ± 0.29 | 1.25 ± 0.65 | ^h 0.88 ± 0.25 |
| | 96 | 0.17 ± 0.41 | ^e 1.30 ± 0.67 | ^h 1.33 ± 0.41 | |

^aStatistical comparisons of mean values were performed using two-way ANOVA followed by Tukey's multiple-comparison test.

^bPMNs: infiltrates of polymorphonuclear cells.

^cSingle infection: Higher proportion of alveolar macrophages in infected- than in non-infected mice, compared to their respective non-infected controls (p<0.001).

^dSingle infection: Higher proportion of alveolar macrophages in E+/I+ than in V+/I+ mice, 24 hpi (p<0.05).

^eRecurrent infection: Higher proportion of alveolar macrophages in infected- than in non-infected mice, compared to their respective non-infected controls (p<0.05).

^fSingle infection: Higher proportion of PMNs in infected- than in non-infected mice, compared to their respective non-infected controls (p<0.0001).

^gSingle infection: Lower proportion of PMNs in E+/I+ than in V+/I+ mice, 1 wpi (p<0.0005).

resistance (R) and elastance (E) in E+/I+ mice compared to their non-infected controls. This is similar to what was observed in V+/I+ mice. Strikingly however, in E+/I+ animals, pulmonary dysfunction remained until 3 weeks post-infection (Figure 2d-f). Similarly, PFT values obtained using a broadband-forced maneuver showed a significant increase in tissue elasticity (H), as well as in parenchymal (G) and airway resistance (Rn), and significantly lower inertance (I) values in E+/I+ compared to E+/- mice, during the first 2 weeks post-infection, and a return to baseline levels 3 wpi (Figure S6, lower panels). Altogether, these results clearly point to higher rigidity of both lung parenchyma and central airways, exacerbated due to the emphysematous background, since the measured increment in all physiology parameters, relative to their respective controls, was higher in E+/I+ than in V+/I+ mice (Figure S6). Indeed, the peak of parenchymal inflammation in E+/I+ mice, measured from most PFT parameters, raised relative to its control (E+/-) levels, and was shifted from 48 hpi to 1 wpi, while the recovery of the PFT parameters back to the level of the emphysematous non-infected E+/- background levels was delayed 2 weeks. Thus, from the standpoint of lung function, the existence of an emphysematous

background exacerbates the intensity and duration of the effects of the NTHi infection.

Consistent with the PFT measurements, visual analysis of micro-CT images revealed higher X-ray density areas in E+/I+ lungs 48 hpi compared to E+/- mice. This increment became more evident 1 wpi, while full recovery of E+/I+ lungs also occurred 3 weeks after NTHi infection (figure 3f). Despite this, radiological signs of inflammation were less well defined in E+/I+ than in V+/I+ mice, maybe due to preexisting alveolar wall degradation caused by elastase activity that reduces bacterial target cell types or tissues. Quantitative analysis of E+/I+ lungs revealed significant differences in the MLVI index compared to E+/- mice, 48 h after infection (Figure 3i), and significantly lower RVB -900 HU values were detected 48 hpi and 1 wpi, consistent with the described inflammatory peak (Figure 3h). These results are clearly reflected in the 3D renders shown in Figure 3j. Bearing these findings in mind, NTHi infection modifies lung physiology and induces parenchymal inflammation regardless of lung status. However, the inflammatory process is longer and more acute in the emphysematous-like background. For completion, expression of *kc* and *tnf-α* pro-inflammatory genes in lung tissue of E+/I+ mice

was higher 24 and 48 hpi than in E+/I- animals, and such increase was restored to basal levels 1 wpi. In addition, expression of the *mmp-2* and *mmp-12* genes in lung tissue of E+/I+ mice was lower at 24 and 48 hpi than in E+/I- animals (**Figure S4**).

The extent of emphysema in histological images of infected lung sections was also analyzed using the MLL, D2, and $R_{\text{alv/tissue}}$ descriptors. All three parameters were higher in E+/I+ than in V+/I+, confirming a clear enlargement of alveolar spaces and, thus, the presence of emphysema (**Figure S2**). No significant differences were found between lobes, showing a homogeneous extent of emphysema across the lung. Caspase-3 staining showed significant increase in apoptotic cell density (Caspase-3⁺/mm²) 24 d after elastase treatment in E+/I+ mice compared to the V+/I+ group (**Figure S3**), pointing to a higher apoptosis rate within the lung parenchyma of animals instilled both with elastase and NTHi.

Conversely, no significant differences in terms of lymphocyte counts were observed between E+/I- and E+/I+ groups. Contrarily, scoring of alveolar macrophages and bronchiolar recruitment of PMNs showed higher numbers in E+/I+ than in E+/I- animals, and scores of PMNs recruitment were higher 24 and 48 hpi, and decreased after 1 wpi. Furthermore, we observed higher alveolar macrophage scoring 24 hpi and lower PMN recruitment 1 wpi in those animals treated with elastase (E+/I+) compared to V+/I+ mice (**Table 1**, upper panels).

Summarizing, these results suggest an increased infectious response caused by NTHi in mice undergoing emphysema lesions promoted by altered expression of pro-inflammatory cytokines and the consequent infiltration of cells with inflammatory activity (macrophages and PMN), which seem to cause longer persistence of parenchymal lesions detected by X-ray imaging, as well as alteration of physiological lung parameters in the E+/I+ animals compared to V+/I+ ones.

Modeling the COPD frequent exacerbator phenotype by NTHi recurrent infection in emphysematous mouse lung

We next reasoned that recurrent NTHi infections in a background of lung emphysema might faithfully recapitulate features of the COPD frequent exacerbator phenotype. The generation of this model (E+/I2+) and its multimodal longitudinal analysis is presented in **Figure 4a**. We inoculated *H. influenzae* Xen21 (day -7) and allowed 1 week for the infection to clear. Then, we performed a second identical inoculation (day 0). In non-emphysematous, re-infected V+/I2+ animals, the

bacterial load measured was almost undetectable 48 h after re-infection, similar to what was observed in singly infected V+/I+ animals. However, clearance after bacterial re-infection was slower in E+/I2+ mice, taking almost 96 h (**Figures 4B and 1b**).

The dynamics of recurrent pulmonary infection by *H. influenzae* were also examined by PFT and micro-CT. Namely, PFT values obtained by single-frequency-forced oscillation displayed lower compliance (C) and increased resistance (R) and elastance (E) during the first 6 weeks after re-infection (V+/I2+), compared to non-infected V+/I2- mice (**Figure 5a**). This trend was similar in those animals with an emphysematous-like background (E+/I2+), which also displayed significantly lower compliance (C) and higher resistance (R) and elastance (E) than E+/I2- mice. However, pulmonary lesions were sustained in E+/I2+ mice up to 9 weeks after re-infection, and full recovery did not occur until week 12 post re-infection (**Figure 5b**). Similarly, pulmonary function values obtained using a broadband-forced maneuver showed a significant increase in tissue elasticity (H), as well as in parenchymal (G) and airway resistance (Rn), and significantly lower tissue inertance (I) values in V+/I2+ and E+/I2+ mice compared to their respective non-infected groups. Functional parameters, as observed in the single-frequency-forced maneuver, displayed the same time recovery gap, i.e. 9 and 12 weeks for V+/I2+ and E+/I2+, respectively (**Figure S7**). These results highlight that recurrent NTHi infection causes chronic pulmonary lesions and delays parenchymal recovery regardless of lung status, although the recovery time needed is longer in the emphysematous lung. In this sense, micro-CT images visual analysis revealed evident higher X-ray density areas both in V+/I2+ and E+/I2+ lungs during the first week after re-infection compared to the non-infected groups, consistent with the inflammatory peak (**Figure 5c-d**). These densely radiopaque areas disappeared in V+/I2+ mice 9 weeks after re-infection, while they subsided in E+/I2+ mice week 12 post re-infection. Summarizing, recurrent NTHi infection elicits a synergistic effect of the pulmonary lesion and reveals circular infection dynamics that compromise lung recovery, further exacerbated by the parenchymal degradation developed in elastase-treated mice E+/I2+.

Likewise, microscopy scoring of lower airway histopathological lesions in samples from V+/I2+ and E+/I2+ groups, euthanized 24, 48, 72, and 96 h after re-infection, showed no differences in terms of PMN recruitment when comparing the V+/I2+ and E+/I2+ groups. Scoring of alveolar macrophages and lymphocytes showed higher numbers in infected than in

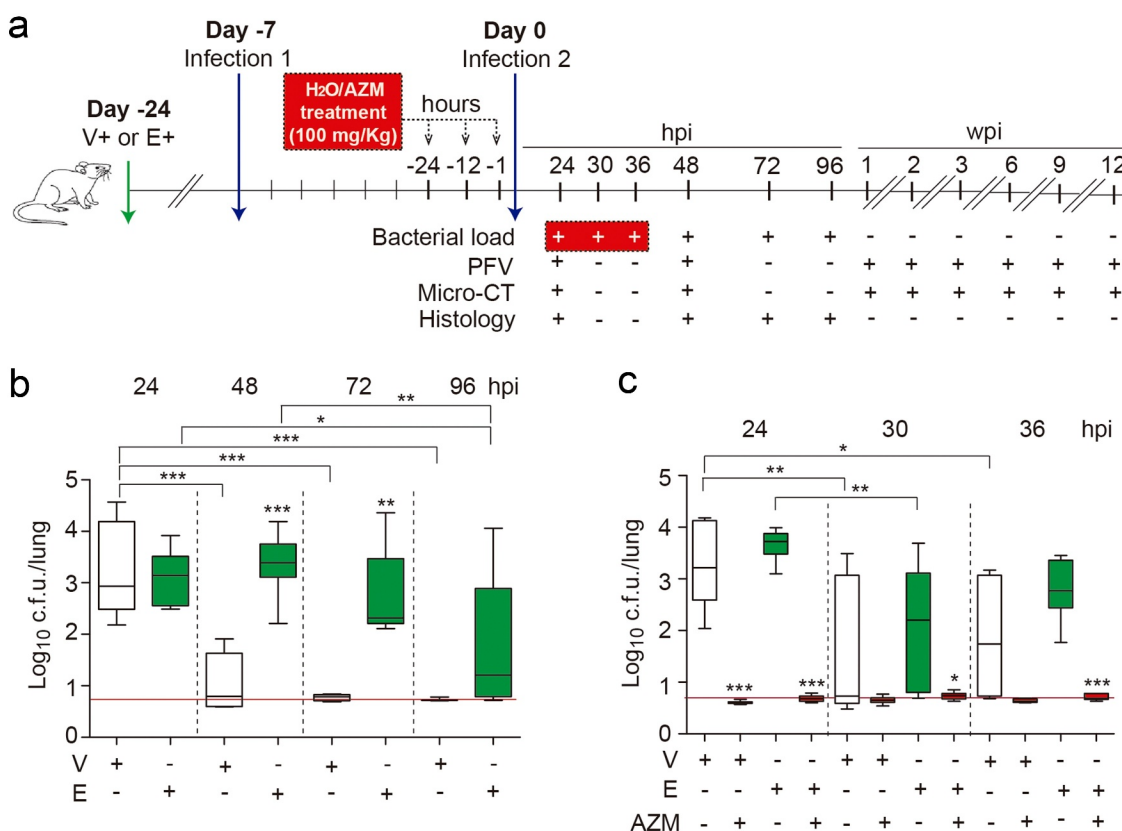


Figure 4. Emphysema mice recurrent pulmonary infection by NTHi, experimental design and analysis of lung bacterial loads. (a) Experimental design: lung emphysema was induced by oropharyngeal instillation of PPE (Day -24). Controls: animals were administered vehicle solution (V+/-) but did not receive elastase (E+/-). Animals were infected with $\sim 10^8$ CFU/mouse of *H. influenzae* Xen21 (Day -7, infection 1). Same animals were infected with $\sim 10^8$ CFU/mouse of *H. influenzae* Xen21 (Day 0, infection 2), V+/- and E+/- groups. Assay types and sampling time points are indicated. (b) Mice were infected as indicated in (a), euthanized 24, 48, 72 and 96 hpi, and bacterial loads quantified in lungs (\log_{10} CFU/lung). Infection took longer to clear in emphysema mice, significant differences were observed between V+ (white) and E+ (green) mice 48 ($p < 0.0001$) and 72 ($p < 0.01$) hpi. V+/- mice: bacterial counts were lower 48, 72 and 96- than 24 hpi ($p < 0.001$). E+/- mice: bacterial counts were lower 96- than 24 and 48 hpi ($p < 0.05$ and $p < 0.01$, respectively). (c) Effect of AZM administration on bacterial loads in NTHi infected mice. AZM (100 mg/kg/dose) was administered oroesophageally as indicated in (a). Control animals were administered water. Bacterial counts were determined 24, 30 and 36 hpi. V+ infected animals: 24 hpi, Xen21 counts were significantly lower in V+/-/AZM than in V+/- animals ($p < 0.0001$). Also, bacterial counts were lower 30 and 36 than 24 hpi ($p < 0.01$ and $p < 0.05$, respectively). E+ infected mice: bacterial counts were lower in E+/-/AZM than in E+/- animals 24 ($p < 0.0001$), 30 ($p < 0.05$) and 36 ($p < 0.0001$) hpi. Also, bacterial counts were lower 30 than 24 hpi ($p < 0.01$). Results are reported as \log_{10} CFU/lung and represented as box plot graphs (lines inside boxes represent median values). Statistical comparisons were performed using one-way ANOVA and Tukey's multiple comparison test. *** $p < 0.001$; ** $p < 0.01$; * $p < 0.05$.

non-infected animal groups. Scoring of lymphocytes was initially low but increased over time in the same manner in both infected groups. Finally, when comparing single and recurrent infection, higher proportion of PMN was observed in E+/- than in E+/- mice, at 48 hpi (Table 1).

In conclusion, our analysis shows that the E+/- phenotype could represent a suitable model system for the COPD frequent exacerbator phenotype, as it displays a longer time for bacterial clearance, together with a synergistic effect of the infectious and emphysematous attacks that produces inflammatory lesions observed to remain in the lung until 12 weeks post re-infection.

Azithromycin clears NTHi infection in a COPD frequent exacerbator mouse model

Antibiotics are indicated in patients with severe COPD who suffer frequent exacerbations despite optimal inhaler therapy, as being beneficial by reducing hospital readmissions and frequency of acute exacerbations [34,35]. Based on its clinical interest, our model was used to assess the efficacy of AZM. The minimal inhibitory concentration (MIC) of AZM for the NTHi Xen21 strain is 4 $\mu\text{g/ml}$. We sought to determine the impact of AZM oroesophageal administration on NTHi recurrent pulmonary infection, by using a regimen

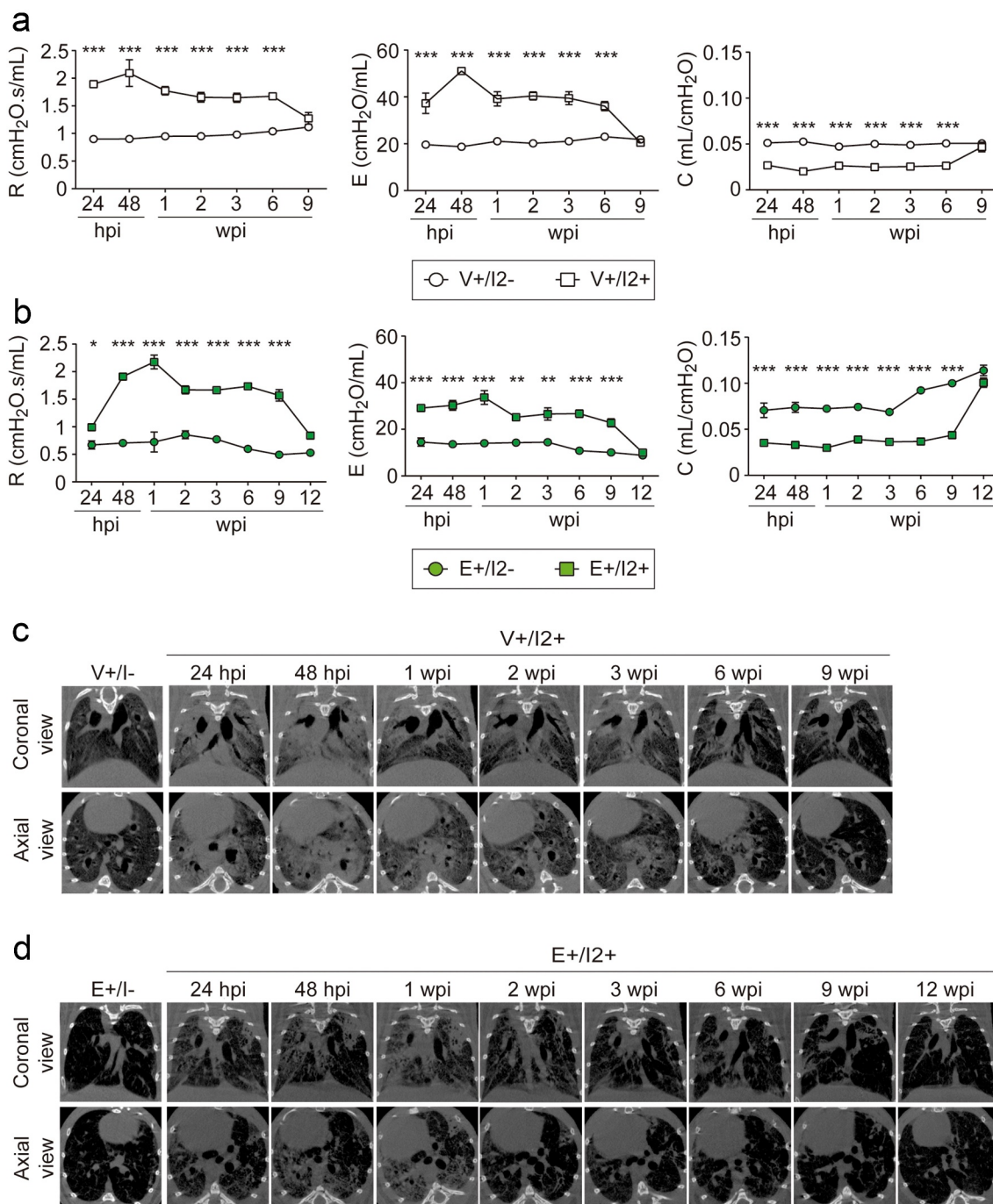


Figure 5. Recurrent NTHi infection exacerbates lung damage and renders chronic lung lesions in mice. CD1 mice were infected with NTHi Xen21 on days -7 and 0 , after instillation of physiological saline solution ($V+/I2+$) or PPE ($E+/I2+$), as indicated in Figure 4a. (a-b) Evolution of physiological parameters at the indicated time points, measured in $V+/I2+$ and $E+/I2+$ mice, in comparison with their respective non-infected groups ($V+/I2-$ and $E+/I2-$). Mice groups: $V+/I2-$ and $E+/I2-$, white and green circles, respectively; $V+/I2+$ and $E+/I2+$, white and green squares, respectively. (a, b) Lung resistance (R , $\text{cmH}_2\text{O}\cdot\text{s}/\text{mL}$), elastance (E , $\text{cmH}_2\text{O}/\text{mL}$) and compliance (C , $\text{mL}/\text{cmH}_2\text{O}$) measured by the single-frequency forced oscillation maneuver. (c, d) Representative micro-CT images ($n = 2$) in the longitudinal section (upper row) and cross-section (bottom row) acquired from the chest of the $V+/I2+$ and $E+/I2+$ mice at the indicated time points. $V+/I-$ and $E+/I-$ animals are shown as controls. Results are shown as mean \pm SEM, statistical differences were analyzed using a two-way ANOVA followed by Bonferroni's post-hoc test. *** $p < 0.001$; ** $p < 0.01$; * $p < 0.05$.

consisting of repeated AZM administrations (Figure 4a), by adapting a previously used approach [36]. The results indicated that this AZM treatment was effective providing clearance of NTHi infection at the three post-infection time points tested when comparing V+/I2+/AZM to V+/I2+, and E+/I2+/AZM to E+/I2+. Such clearing effect was independent of previous emphysema development (Figure 4c). AZM has dual antimicrobial and anti-inflammatory properties [37]. Histopathology score was not performed on AZM-treated groups precluding us from assessing its effect on leukocyte recruitment. Nevertheless, we quantified the expression of *kc* and *tnf- α* pro-inflammatory genes in lung tissue of E+/I2+ mice upon AZM treatment, and observed a decrease to basal levels comparable to those in uninfected animals (Figure S8). AZM cleared NTHi infection; therefore, the observed effect may be the outcome of both AZM immunomodulatory and antibiotic effects.

Discussion

Understanding the nature and frequency of COPD exacerbations is instrumental to identify individuals at high risk for such events, and for the delineation of specific clinical phenotypes. Four phenotypes of exacerbations have been described: bacterial, viral, inflammatory (eosinophilic), and pauci-inflammatory, being more than 50% of them of microbial nature. Bacterial exacerbations can be explained by (i) the “fall and rise” hypothesis, suggesting a primary chronic bronchial infection as a result of impaired local defenses. The increase in bronchial bacterial load and associated increase in inflammation in a chronically infected patient may cause the symptoms of exacerbation; (ii) newly acquired infecting strains against which no immune protection exists may explain the occurrence of an exacerbation; (iii) a viral infection may impair the local defenses thus facilitating bacterial infection [5]. Furthermore, the Global Initiative for Chronic Obstructive Lung Disease (GOLD) therapeutic strategy requires a history of two or more exacerbations in the previous year as a key component to define frequent exacerbators [38,39]. In this context, we addressed the need for a disease model of such frequent exacerbator phenotype with bacterial origin, by presenting a novel mouse model of recurrent bacterial pulmonary infections in an emphysematous lung. Several groups have established animal models of bacterial exacerbation in COPD [15,40,41], and cigarette smoke and elastase/LPS treatment have been shown to exacerbate the inflammatory responses to NTHi in mice [13,14,16,19–21]. However, to the best of our knowledge, our model

recapitulates, for the first time, the inflammatory component of the frequent exacerbator situation observed in COPD patients, by using two recurrent bacterial inoculations in a damaged murine lung undergoing emphysema lesions. From a mechanistic perspective, we may recall a situation half-way between the above cited “fall and rise” and newly infecting strain hypotheses, by generating recurrent infection by repeated inoculation of clonal bacteria.

The standard techniques used to evaluate infection in preclinical settings, i.e. microbial load quantification in homogenized tissues and microscopic observation, are severely limited by their invasive character, thus precluding the longitudinal evaluation of the disease in the same animal, and requiring sampling of high number of animals. Conversely, X-ray micro-CT imaging allows noninvasive longitudinal monitoring of disease progression. This technique was previously applied to the study of invasive pulmonary aspergillosis, cryptococcosis, *S. aureus* pneumonia, or lung lesions by *Streptococcus pyogenes* [23,28,42–44], and also to track emphysematous lesions over time in living mice and evaluate the progression of the associated alveolar destruction [24,27]. Indeed, the extent of emphysema in a mouse lung has been shown to correlate with the mean X-ray intensity, the prevalence of low-density areas, and/or the total lung volume. More relevant to our work, this imaging approach has been previously used to characterize a model of exacerbation in COPD, generated by administering a single dose of LPS into the trachea of mice with established emphysematous lung disease instigated by prior exposure to elastase [45]. Here, we go one step further, by using micro-CT to evaluate disease progression in a model consisting of a single or recurrent *H. influenzae* pulmonary infection in an emphysematous mouse lung, as a means of modeling COPD baseline and frequent exacerbation. Our quantitative micro-CT-based results show that the models of single (E+/I+), and especially of recurrent (E+/I2+) infection display clear radiological signs of lung inflammation that are higher in intensity and take longer to clear (3 weeks in the E+/I+ and 12 weeks in the E+/I2+ model) than the control model of infection on a non-emphysematous lung (V+/I+), clearing all radiological signs of inflammation in 1 week.

COPD clinical management normally includes pulmonary function tests, to measure the amount of air inhaled and exhaled, and whether the lungs deliver enough oxygen to the blood (spirometry, measurement of lung volumes and diffusing capacity, 6-minute walk test, pulse oximetry). Accordingly, we quantitatively characterized lung function in our mouse models

using passive tests of pulmonary function. By using both a single frequency and a more complex broad-band-forced oscillation model, we quantified the effect of the infectious process in the function of the lungs, observing in all cases (V+/I+, E+/I+, V+/I2+, E+/I2+), temporal trends in the main parameters tracked that closely parallel those observed by micro-CT imaging. This highlights the complementary value of both techniques that faithfully capture the lung damage caused by the inflammatory and elastolytic damage inflicted on the lungs, both at radiological and physiological levels. To further correlate our radiological findings with *in situ* measurements of inflammation, we measured the expression of pro-inflammatory cytokines associated with bacterial infection and inflammatory cell recruitment, supported by previous studies reporting how PMNs play key roles in parenchymal elastolytic degradation and actively contribute to emphysema progression [46,47]. These results suggest that the inflammatory response takes place immediately after instillation of NTHi and correlates over time with the development of inflammation areas on radiographic images as well as their effect on pulmonary function. In summary, our findings highlight the potential of micro-CT to perform longitudinal studies and provide accurate information on emphysema progression and inflammation development and clearance.

Another interesting outcome of this study is that recovery times for bacterial load clearance from the murine lungs and airways return to baseline symptoms, were uncoupled, and such uncoupling is different and amplified after recurrent infection. Thus, bacteria are cleared 48 h post-single infection but return to baseline symptoms takes up to 3 weeks in the exacerbator (E+/I+) model; even more, bacteria are cleared 96 h post-recurrent infection and return to baseline symptoms takes up to 12 weeks in the frequent exacerbator (E+/I2+) model. When translating into humans, patients recover to baseline symptoms after 7 d in half of exacerbations, but in about 14% of events patients do not return to baseline symptoms within 35 d of onset, and in a small proportion, symptoms never return to the baseline level. In fact, ~30% of exacerbated patients are seen again and possibly readmitted with another event within 8 weeks, and ~20% of moderate-severe COPD patients followed-up after exacerbation have a recurrent event within 50 d of the first one. Thus, an initial exacerbation increases susceptibility to a subsequent one, and patients with a history of frequent exacerbations have increased airway inflammation likely contributing to disease progression [2]. Overall, we put forward the notion that the E+/I2+ phenotype may nicely emulate several features of the

COPD frequent exacerbator phenotype. The observed delays in both bacterial clearance and inflammatory lung recovery after re-infection, compared to single infection and non-infected control groups, are aligned with clinical observations, and with the notion of recurrent infection contributing to disease progression in a circular manner (Figure 6, upper graphs).

Our multimodal approach based on quantifying bacterial and host lung parameters, has shown to be highly complementary. However, we acknowledge several drawbacks and considerations. First, we initially considered bioluminescence imaging to obtain longitudinal information on the extent of bacterial load, but could not be reliably used. Bioluminescence was previously used by other groups to monitor NTHi infection within the nasopharynx, eustachian tubes and middle ear of chinchilla after intranasal and transbullar infections [48–50], but did not allow direct monitoring of bacterial movement from the nasopharynx to the middle ear in a *Junbo* mouse model of otitis media due to insufficient signal [33]. Bioluminescence monitoring of lung infection renders dissimilar results depending on mouse models, pathogens and strains [51]. Here, correlation of bioluminescence signal with bacterial loads was poor, maybe due to spread and dilution of the non-multiplying inoculum rendering insufficient signal for an imaging of the lower airways *in vivo*. This type of limitation was previously reported for *S. pneumoniae* and *Pseudomonas aeruginosa* [52,53]. Second, the number of recurrent infections in the same animal may be a limiting factor. Here, we performed two identical recurrent infections 1 week apart. After the second infection, the bacterial load recovered 24 hpi was lower than after the first one, maybe due to the increased animal weight or immune system insensitivity. This issue could be amplified in subsequent infections. Third, the quantification of alveolar cell destruction by Caspase-3 immunostaining showed a trend, but not a significant difference between the V+/I- and E+/I- groups. This is most likely due to the relatively low number of animals analyzed (n = 5), and the analysis time point. Indeed, 24 d after elastase instillation, which is an appropriate time point to evaluate the extent of emphysematous lesion, might be a late time to evaluate the level of alveolar destruction by means of the quantification of apoptotic cells. A future time course assay, including earlier times would allow investigating the apoptotic effect of elastase on alveolar cells from the time of elastase instillation on. Fourth, elastase-induced emphysema, which we acknowledge may have limitations when resembling the pathology seen in COPD, did not allow consistent sampling of bronchoalveolar lavage fluid, impairing the

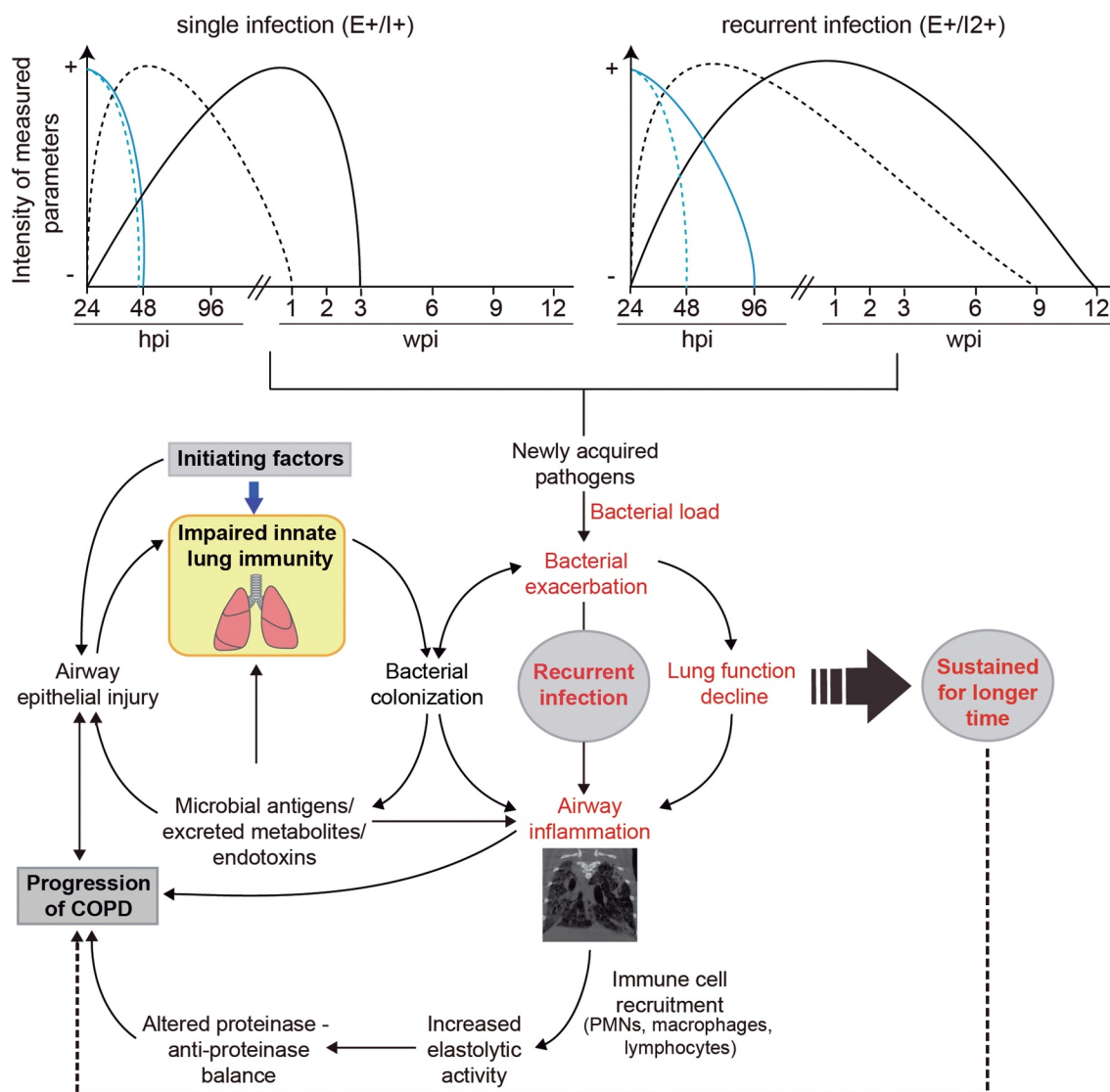


Figure 6. A disease model based on murine emphysematous lung recurrent bacterial infection in the context of the COPD vicious circle hypothesis. Alterations in innate defenses induced by inhalational exposure due to cigarette or biomass smoke allow pathogenic bacteria initiating the endless vicious circle that contributes to disease progression. By modeling increased elastolytic activity by elastase administration and combined use of longitudinal approaches, we observed that newly acquired opportunistic pathogenic bacteria contribute to the decline of pulmonary function and to airway inflammation. Respiratory parameters return to the baseline after bacterial clearance, but such return is much slower than bacterial clearance as such, and this delay is further amplified in the damaged lungs (single infection summary, upper left representation: E+/I+, continuous lines; V+/I+, dashed lines; bacterial load, blue lines; PFT and X-ray data, black lines). Recurrent infection exacerbates such gaps, heavily increasing lung recovery times, i.e. from 3 to 12 weeks after re-infection of emphysema lungs (recurrent infection summary, upper right representation: E+/I2+, continuous lines; V+/I2+, dashed lines; bacterial load, blue lines; PFT and X-ray data, black lines). This E+/I2+ situation may emulate features of the COPD frequent exacerbator phenotype.

analysis of inflammatory cells present in this type of samples. This could relate to the use of CD1 mice, in contrast to previous studies exposing C57BL/6 animals to LPS/elastase [19,45]. Along these lines, the choice of murine models and procedures to generate COPD-type lesions is likely to be a key factor in some aspects of the outcome. In fact, our data regarding bacterial load align nicely with those presented by Pang and coauthors [16], who observed that NTHi pulmonary clearance

was impaired in elastase-treated mice. This is in conflict with Gaschler and coauthors [21], who observed accelerated clearance of NTHi from cigarette smoke-exposed mice. This discrepancy could be due to a higher NTHi-specific IgA in the cigarette smoke animals, or even to an inhibitory/cytotoxic effect of the cigarette smoke on NTHi. Finally, our decision to terminate the experiment at 12 weeks was based on the observation that at that time, we could not see

significant differences between double infected (E+/I2+) and non-infected (E+/I2-) animals, based on the PFT values and a qualitative visual examination of the micro-CT images. Therefore, we focused only in the short-term effect of emphysema in the duration and strength of the infection, monitored after each infectious attack, but not in the long-term effect of the exacerbation on the underlying emphysematous lung. It would be interesting to extend the study to look at the long-term effects of the infection on the baseline emphysema. The expected results of such a long-term study, based on our preliminary results, point to an exacerbation of emphysema in mice that undergo both NTHi infection and emphysema, compared to the non-infected emphysematous mice. This observation agrees with what is reported in the literature after LPS administration in elastase-treated mice [45].

To conclude, the information presented here is integrated in the so-called COPD vicious-circle hypothesis [11], where the gradual lung damage and loss of function are consequences of successive rounds of microbial dysbiosis with anomalous inflammation, where new strains of opportunistic bacteria may account for about one-half of exacerbations. E+/I2+ modeled increased elastolytic activity and recurrent bacterial infection. This way, and by comparing E+/I2+ data with those obtained from E+/I+ and V+/I2+ animal groups through time, we could model the deleterious impact of recurrent lung infection, by sustaining bacterial load, lung function decline, and airway inflammation for longer time (Figure 6). Currently, COPD patients and their physicians face significant clinical challenges, including determining the bases for identifying the biological and clinical implications of the presence of pathogenic bacteria in the airways according to the COPD phenotype, next to exploring suitable treatments. Aligned with those needs, the mouse model presented here aims to provide an *in vivo* tool to facilitate investigating the COPD frequent exacerbator phenotype.

Acknowledgments

We thank Dr. Montserrat Barberán, Facultad de Veterinaria, Universidad de Zaragoza, Spain, for sample processing and scoring of histopathology lesions. This work has been funded by grants from MICIU (UE FEDER) SAF2015-66520-R, RTI2018-096369-B-I00, and RED2018-102469-T, from Health Department, Regional Navarra Govern, Spain, reference 03/2016, and from SEPAR 31/2015 to J.G.; from MICIU (UE FEDER) RTI2018-094494-B-C222 to C.O.S; from University, Innovation and Digital Transformation Department, Regional Navarra Govern, Spain, reference PC150-151-152 to J.G. and C.O.S. CIBER is an initiative from Instituto de Salud Carlos III (ISCIII), Madrid, Spain.

Disclosure of potential conflicts of interest

The authors declare no competing (financial or non-financial) interests.

Funding

This work was supported by the Departamento de Universidad, Innovación y Transformación Digital, Gobierno de Navarra [PC150-151-152]; Ministerio de Ciencia, Innovación y Universidades (MICIU), Gobierno de España [RTI2018-096369-B-I00]; MICIU, Gobierno de España [RED2018-102469-T]; MICIU, Gobierno de España [SAF2015-66520-R]; MICIU, Gobierno de España [RTI2018-094494-B-C222]; Departamento de Salud, Gobierno de Navarra [03/2016]; Sociedad Española de Neumología y Cirugía Torácica [31/2015].

ORCID

Begoña Euba  <http://orcid.org/0000-0001-5620-596X>
Junkal Garmendia  <http://orcid.org/0000-0002-7440-2737>

References

- [1] Celli BR, Wedzicha JA. Update on clinical aspects of chronic obstructive pulmonary disease. *N Engl J Med.* 2019;381(13):1257–1266. Available from: <https://www.ncbi.nlm.nih.gov/pubmed/31553837>
- [2] Wedzicha JA, Seemungal TA. COPD exacerbations: defining their cause and prevention. *Lancet.* 2007;370(9589):786–796. Available from: <https://www.ncbi.nlm.nih.gov/pubmed/17765528>
- [3] Hurst JR, Vestbo J, Anzueto A, et al. Susceptibility to exacerbation in chronic obstructive pulmonary disease. *N Engl J Med.* 2010;363(12):1128–1138. Available from: <https://www.ncbi.nlm.nih.gov/pubmed/20843247>
- [4] Waeijen-Smit K, Houben-Wilke S, DiGiandomenico A, et al. Unmet needs in the management of exacerbations of chronic obstructive pulmonary disease. *Intern Emerg Med.* 2021;16(1):1–11.
- [5] Lopez-Campos JL, Miravittles M, De La Rosa Carrillo D, et al. Current challenges in chronic bronchial infection in patients with chronic obstructive pulmonary disease. *J Clin Med.* 2020;9(6):1639. Available from: <https://www.ncbi.nlm.nih.gov/pubmed/32481769>
- [6] Ahearn CP, Gallo MC, Murphy TF. Insights on persistent airway infection by non-typeable *Haemophilus influenzae* in chronic obstructive pulmonary disease. *Pathog Dis.* 2017;75(4):75.
- [7] Chin CL, Manzel LJ, Lehman EE, et al. *Haemophilus influenzae* from patients with chronic obstructive pulmonary disease exacerbation induce more inflammation than colonizers. *Am J Respir Crit Care Med.* 2005;172(1):85–91.
- [8] Duell BL, Su YC, Riesbeck K. Host-pathogen interactions of nontypeable *Haemophilus influenzae*: from commensal to pathogen. *FEBS Lett.* 2016;590

- (21):3840–3853. Available from: <https://www.ncbi.nlm.nih.gov/pubmed/27508518>
- [9] Look DC, Chin CL, Manzel LJ, et al. Modulation of airway inflammation by *Haemophilus influenzae* isolates associated with chronic obstructive pulmonary disease exacerbation. *Proc Am Thorac Soc.* 2006;3(6):482–483.
- [10] Murphy TF, Brauer AL, Schiffmacher AT, et al. Persistent colonization by *Haemophilus influenzae* in chronic obstructive pulmonary disease. *Am J Respir Crit Care Med.* 2004;170(3):266–272. Available from: <http://www.ncbi.nlm.nih.gov/pubmed/15117742>
- [11] Rangelov K, Sethi S. Role of infections. *Clin Chest Med.* 2014;35(1):87–100. Available from: <https://www.ncbi.nlm.nih.gov/pubmed/24507839>
- [12] Mirza S, Benzo R. Chronic obstructive pulmonary disease phenotypes: implications for care. *Mayo Clin Proc.* 2017;92(7):1104–1112. Available from: <https://www.ncbi.nlm.nih.gov/pubmed/28688465>
- [13] Ganesan S, Comstock AT, Kinker B, et al. Combined exposure to cigarette smoke and nontypeable *Haemophilus influenzae* drives development of a COPD phenotype in mice. *Respir Res.* 2014;15(1):11. Available from: <https://www.ncbi.nlm.nih.gov/pubmed/24495712>
- [14] Herr C, Han G, Li D, et al. Combined exposure to bacteria and cigarette smoke resembles characteristic phenotypes of human COPD in a murine disease model. *Exp Toxicol Pathol.* 2015;67(3):261–269. Available from: <https://www.ncbi.nlm.nih.gov/pubmed/25601416>
- [15] Perez-Rial S, Giron-Martinez A, Peces-Barba G. Animal models of chronic obstructive pulmonary disease. *Arch Bronconeumol.* 2015;51(3):121–127. Available from: <https://www.ncbi.nlm.nih.gov/pubmed/25201221>
- [16] Pang B, Hong W, West-Barnette SL, et al. Diminished ICAM-1 expression and impaired pulmonary clearance of nontypeable *Haemophilus influenzae* in a mouse model of chronic obstructive pulmonary disease/emphysema. *Infect Immun.* 2008;76(11):4959–4967. Available from: <https://www.ncbi.nlm.nih.gov/pubmed/18794286>
- [17] Starkey MR, Jarnicki AG, Essilfie A-T, et al. Murine models of infectious exacerbations of airway inflammation. *Curr Opin Pharmacol.* 2013;13(3):337–344.
- [18] Fernandez-Calvet A, Rodriguez-Arce I, Almagro G, et al. Modulation of *Haemophilus influenzae* interaction with hydrophobic molecules by the VacJ/MlaA lipoprotein impacts strongly on its interplay with the airways. *Sci Rep.* 2018;8(1):6872.
- [19] Ganesan S, Faris AN, Comstock AT, et al. Elastase/LPS-exposed mice exhibit impaired innate immune responses to bacterial challenge: role of scavenger receptor A. *Am J Pathol.* 2012;180(1):61–72. Available from: <https://www.ncbi.nlm.nih.gov/pubmed/22079429>
- [20] Gaschler GJ, Skrtic M, Zavitz CC, et al. Bacteria challenge in smoke-exposed mice exacerbates inflammation and skews the inflammatory profile. *Am J Respir Crit Care Med.* 2009;179(8):666–675. Available from: <http://www.ncbi.nlm.nih.gov/pubmed/19179487>
- [21] Gaschler GJ, Zavitz CCJ, Bauer CMT, et al. Mechanisms of clearance of nontypeable *Haemophilus influenzae* from cigarette smoke-exposed mouse lungs. *Eur Respir J.* 2010;36(5):1131–1142. Available from: <http://erj.ersjournals.com/content/36/5/1131.abstract>
- [22] Wang D, Wang Y, Liu YN. Experimental pulmonary infection and colonization of *Haemophilus influenzae* in emphysematous hamsters. *Pulm Pharmacol Ther.* 2010;23(4):292–299. Available from: <https://www.ncbi.nlm.nih.gov/pubmed/20211751>
- [23] Poelmans J, Hillen A, Vanherp L, et al. Longitudinal, *in vivo* assessment of invasive pulmonary aspergillosis in mice by computed tomography and magnetic resonance imaging. *Lab Invest.* 2016;96(6):692–704. Available from: <https://www.ncbi.nlm.nih.gov/pubmed/27019389>
- [24] Artaechevarria X, Blanco D, De Biurrun G, et al. Evaluation of micro-CT for emphysema assessment in mice: comparison with non-radiological techniques. *Eur Radiol.* 2011;21(5):954–962. Available from: <https://www.ncbi.nlm.nih.gov/pubmed/20953986>
- [25] Artaechevarria X, Munoz-Barrutia A, Ortiz-de-solorzano C. Combination strategies in multi-atlas image segmentation: application to brain MR data. *IEEE Trans Med Imaging.* 2009;28(8):1266–1277. Available from: <https://www.ncbi.nlm.nih.gov/pubmed/19228554>
- [26] Artaechevarria X, Perez-Martin D, Ceresa M, et al. Airway segmentation and analysis for the study of mouse models of lung disease using micro-CT. *Phys Med Biol.* 2009;54(22):7009–7024. Available from: <https://www.ncbi.nlm.nih.gov/pubmed/19887716>
- [27] Munoz-Barrutia A, Ceresa M, Artaechevarria X, et al. Quantification of lung damage in an elastase-induced mouse model of emphysema. *Int J Biomed Imaging.* 2012;2012:734734. Available from <https://www.ncbi.nlm.nih.gov/pubmed/23197972>
- [28] Poelmans J, Himmelreich U, Vanherp L, et al. A multimodal imaging approach enables *in vivo* assessment of antifungal treatment in a mouse model of invasive pulmonary aspergillosis. *Antimicrob Agents Chemother.* 2018;62(7):62. Available from: <https://www.ncbi.nlm.nih.gov/pubmed/29760132>
- [29] Löffek S, Schilling O, Franzke C-W. Series “matrix metalloproteinases in lung health and disease”: biological role of matrix metalloproteinases: a critical balance. *Eur Respir J.* 2011;38(1):191–208.
- [30] Koo H-K, Hong Y, Lim MN, et al. Relationship between plasma matrix metalloproteinase levels, pulmonary function, bronchodilator response, and emphysema severity. *Int J Chron Obstruct Pulmon Dis.* 2016;11:1129–1137.
- [31] Lopez-Lopez N, Euba B, Hill J, et al. *Haemophilus influenzae* glucose catabolism leading to production of the immunometabolite acetate has a key contribution to the host airway–pathogen interplay. *ACS Infect Dis.* 2020;6(3):406–421. Available from: <https://www.ncbi.nlm.nih.gov/pubmed/31933358>
- [32] Molerés J, Fernandez-Calvet A, Ehrlich RL, et al. Antagonistic pleiotropy in the bifunctional surface protein FadL (OmpP1) during adaptation of *Haemophilus influenzae* to chronic lung infection associated with

- chronic obstructive pulmonary disease. *MBio*. 2018;9(5). doi:10.1128/mBio.01176-18.
- [33] Hood D, Moxon R, Purnell T, et al. A new model for non-typeable *Haemophilus influenzae* middle ear infection in the *Junbo* mutant mouse. *Dis Model Mech*. 2016;9(1):69–79. Available from: <https://www.ncbi.nlm.nih.gov/pubmed/26611891>
- [34] Al-Hasan MN, Al-Jaghbeer MJ. Use of antibiotics in chronic obstructive pulmonary disease: what is their current role in older patients? *Drugs Aging*. 2020;37(9):627–633. Available from: <https://www.ncbi.nlm.nih.gov/pubmed/32691330>
- [35] Plusa T. Azithromycin in the treatment of patients with exacerbation of chronic obstructive pulmonary disease. *Pol Merkur Lek* 2020; 48:65–68. Available from: <https://www.ncbi.nlm.nih.gov/pubmed/32218410>.
- [36] Euba B, Molerés J, Viadas C, et al. Relationship between azithromycin susceptibility and administration efficacy for nontypeable *Haemophilus influenzae* respiratory infection. *Antimicrob Agents Chemother*. 2015;59(5):2700–2712. Available from: <http://www.ncbi.nlm.nih.gov/pubmed/25712355>
- [37] Huckle AW, Fairclough LC, Todd I. Prophylactic antibiotic use in COPD and the potential anti-inflammatory activities of antibiotics. *Respir Care*. 2018;63(5):609–619. Available from: <https://www.ncbi.nlm.nih.gov/pubmed/29463692>
- [38] Labaki WW, Martínez FJ. Time to understand the infrequency of the frequent exacerbator phenotype in COPD. *Chest*. 2018;153(5):1087–1088. Available from: <https://www.ncbi.nlm.nih.gov/pubmed/29731034>
- [39] Le Rouzic O, Roche N, Cortot AB, et al. Defining the “frequent exacerbator” phenotype in COPD: a hypothesis-free approach. *Chest*. 2018;153(5):1106–1115. Available from: <https://www.ncbi.nlm.nih.gov/pubmed/29054347>
- [40] Gaschler GJ, Bauer CMT, Zavitz CCJ, et al. Animal models of chronic obstructive pulmonary disease exacerbations. *Contrib Microbiol*. 2007;14:126–141. Available from <https://www.ncbi.nlm.nih.gov/pubmed/17684337>
- [41] Wright JL, Cosio M, Churg A. Animal models of chronic obstructive pulmonary disease. *Am J Physiol Lung Cell Mol Physiol*. 2008;295(1):L1–15. Available from: <https://www.ncbi.nlm.nih.gov/pubmed/18456796>
- [42] Mason WJ, Skaar EP. Assessing the contribution of heme-iron acquisition to *Staphylococcus aureus* pneumonia using computed tomography. *PLoS One*. 2009;4(8):e6668. Available from: <https://www.ncbi.nlm.nih.gov/pubmed/19688098>
- [43] Minami M, Sobue S, Ichihara M, et al. Analysis of the pathological lesions of the lung in a mouse model of cutaneous infection with *Streptococcus pyogenes*. *Pathol Int*. 2012;62(2):99–104. Available from: <https://www.ncbi.nlm.nih.gov/pubmed/22243779>
- [44] Vanherp L, Ristani A, Poelmans J, et al. Sensitive bioluminescence imaging of fungal dissemination to the brain in mouse models of cryptococcosis. *Dis Model Mech*. 2019;12(6): Available from <https://www.ncbi.nlm.nih.gov/pubmed/31101657>
- [45] Kobayashi S, Fujinawa R, Ota F, et al. A single dose of lipopolysaccharide into mice with emphysema mimics human chronic obstructive pulmonary disease exacerbation as assessed by micro-computed tomography. *Am J Respir Cell Mol Biol*. 2013;49(6):971–977. Available from: <https://www.ncbi.nlm.nih.gov/pubmed/23822858>
- [46] Jasper AE, Sapey E, Walton GMMWJ. Understanding the role of neutrophils in chronic inflammatory airway disease. *F1000Res*. 2019;8:F1000Faculty Rev–557.
- [47] Meijer M, Fj Rgt VO. Neutrophils and emerging targets for treatment in chronic obstructive pulmonary disease. *Expert Rev Clin Immunol*. 2013;9(11):1055–1068.
- [48] Bookwalter JE, Jurcisek JA, Gray-Owen SD, et al. A carcinoembryonic antigen-related cell adhesion molecule 1 homologue plays a pivotal role in nontypeable *Haemophilus influenzae* colonization of the chinchilla nasopharynx via the outer membrane protein P5-homologous adhesin. *Infect Immun* [Internet] 2008; 76(1):48–55. Available from: <https://www.ncbi.nlm.nih.gov/pubmed/17938212>
- [49] Mason KM, Munson JRS, Bakaletz LO. A mutation in the *sap* operon attenuates survival of nontypeable *Haemophilus influenzae* in a chinchilla model of otitis media. *Infect Immun*. 2005;73(1):599–608. Available from: <https://www.ncbi.nlm.nih.gov/pubmed/15618200>
- [50] Novotny LA, Mason KM, Bakaletz LO. Development of a chinchilla model to allow direct, continuous, biophotonic imaging of bioluminescent nontypeable *Haemophilus influenzae* during experimental otitis media. *Infect Immun*. 2005;73(1):609–611. Available from: <https://www.ncbi.nlm.nih.gov/pubmed/15618201>
- [51] Avci P, Karimi M, Sadasivam M, et al. *In vivo* monitoring of infectious diseases in living animals using bioluminescence imaging. *Virulence*. 2018;9(1):28–63. Available from: <https://www.ncbi.nlm.nih.gov/pubmed/28960132>
- [52] Henken S, Bohling J, Ogunniyi AD, et al. Evaluation of biophotonic imaging to estimate bacterial burden in mice infected with highly virulent compared to less virulent *Streptococcus pneumoniae* serotypes. *Antimicrob Agents Chemother*. 2010;54(8):3155–3160. Available from: <https://www.ncbi.nlm.nih.gov/pubmed/20530224>
- [53] Munder A, Wolbeling F, Klockgether J, et al. *In vivo* imaging of bioluminescent *Pseudomonas aeruginosa* in an acute murine airway infection model. *Pathog Dis*. 2014;72(1):74–77. Available from: <https://www.ncbi.nlm.nih.gov/pubmed/24833236>